Near-Field Enhanced Negative Luminescent Refrigeration

Kaifeng Chen,[1] Parthiban Santhanam,[2] and Shanhui Fan[2,*]
[1]Department of Applied Physics, Stanford University, Stanford, California 94305, USA
[2]Department of Electrical Engineering, Ginzton Laboratory, Stanford University, Stanford, California 94305, USA
(Received 22 March 2016; revised manuscript received 5 July 2016; published 18 August 2016)

We consider a near-field enhanced negative luminescent refrigeration system made of a polar material supporting surface-phonon polariton resonances and a narrow-band-gap semiconductor under a reverse bias. We show that in the near-field regime, such a device yields significant cooling power density and a high efficiency close to the Carnot limit. In addition, the performance of our system still persists even in the presence of strong nonidealities such as Auger recombination and sub-band-gap thermal radiation from free carriers.

DOI: 10.1103/PhysRevApplied.6.024014

I. INTRODUCTION

When a semiconductor p-n junction is under external bias, the expectation value of the photon energy per mode above the band gap satisfies the Bose-Einstein distribution [1]

$$\Theta(\omega, T, V) = \frac{\hbar\omega}{e^{\frac{\hbar\omega - qV}{k_B T}} - 1}, \tag{1}$$

where $\hbar$ is the reduced Planck's constant, ω is the angular frequency, q is the magnitude of the electron's charge, V is the external bias, k_B is the Boltzmann constant, and T is the temperature of the semiconductor. Thus, in the presence of a negative bias (i.e., $V < 0$), the semiconductor p-n junction emits fewer photons as compared to the same system at thermal equilibrium with $V = 0$. In such a situation, as far as thermal radiation properties are concerned, one can equivalently describe the semiconductor as having an apparent temperature lower than its real temperature [2–8]. This effect, i.e., the suppression of thermal radiation from a semiconductor p-n junction by applying a negative bias, is commonly referred to as "negative luminescence" and has applications such as cold shields for IR detectors [9], radiometric reference sources [10], and dynamic infrared scene projectors [10].

One potential application of negative luminescence is in the area of solid-state cooling [11,12]. In Ref. [11], Berdahl considered two semiconductor objects having different temperatures undergoing radiative thermal exchange between them and showed theoretically that a net heat flow from the cold to the hot object is possible when the hot object is under a negative bias. His calculation was mostly carried out in the far-field regime, in which the separation between the two bodies is much greater than all wavelengths relevant to electromagnetic heat transfer between the bodies. In such a case, the achievable power density for cooling is fundamentally limited by the Stefan-Boltzmann law. He also noted the potential enhancement in the near field due to the high index of the semiconductors.

In recent years, there have been significant theoretical [13–22] and experimental [23–27] efforts in exploring near-field heat transfer, through which the power density can far exceed the far-field limit. Motivated by these efforts, in this paper we examine the concept of negative luminescent refrigeration in the near-field regime. We consider a configuration as shown in Fig. 1, where a narrow-band-gap semiconductor p-n junction under negative bias is placed in close proximity to a dielectric material supporting phonon-polariton resonances. We show that operation in the near-field regime results in significant enhancement of both the power density and coefficient of performance for negative luminescent refrigeration. Our work differs from Ref. [11] in two essential aspects. First of all, in our system, the near-field heat transfer is enhanced through the use of surface-phonon polaritons, which give rise to a much larger enhancement not limited by the indices of the semiconductors. Second, we also provide a quantitative evaluation of the impacts of nonidealities in the near-field regime, which was not carried out in Ref. [11].

This work is connected to but also differs significantly from a recent publication [28]. Reference [28] considered a related cooling scheme exploiting radiative energy exchange between a colder semiconductor p-n junction body under external bias and another hotter thermal body. A positive bias was applied to the colder semiconductor p-n junction body to extract heat from the cold to the hot body. In the scheme of Ref. [28], since the electric bias in this case is applied to the cold side, the cooling power is limited by the Auger recombination and cannot reach the radiative limit. However, as we see in the following sections, the negative luminescent scheme eliminates this

*shanhui@stanford.edu

constraint since the electrical bias in this case is applied to the hot side, and, therefore, Auger recombination is no longer a direct heating process on the cold side.

The rest of the paper is organized as follows: In Sec. II, we briefly review the concept of negative luminescent refrigeration. In Sec. III, we present the results of a system consisting of mercury cadmium telluride (MCT) and hexagonal boron nitride (*h*-BN). We conclude in Sec. IV.

II. BRIEF REVIEW OF NEGATIVE LUMINESCENT REFRIGERATION

We start by a brief review of the concept of negative luminescent refrigeration. Following Ref. [11], we consider the configuration shown in Fig. 1, where body 1 at T_1 is in thermal exchange with body 2 at temperature T_2. Body 2 is made of a semiconductor with band-gap energy E_g. In this configuration, the device forming body 2 can be fabricated in a process where one first fabricates a diode on a substrate. The substrate is then removed, and finally a metal layer is deposited on the diode to act as the mirror. We assume that $T_1 < T_2$. The objective of negative luminescent refrigeration is to extract heat from body 1, in spite of the fact that it has a lower temperature, by applying a negative bias $V < 0$ to the semiconductor body 2. We assume a device configuration as shown in Fig. 1 where the semiconductor region is intrinsic, and external bias is applied through two heavily doped regions labeled P^+ and N^+, respectively. The convention for the signs is chosen such that a positive current corresponds to the flow of positive charge from P^+ anode through the intrinsic region to the N^+ cathode. The negative bias then generates a negative current I. The total electric power that is used to drive the two-body system is then $I \times V$.

A cooling device as such is characterized by its cooling power density and its efficiency. The cooling power density P is defined as the net electromagnetic power per unit area that flows from body 1 to 2. The efficiency of a device is characterized by the coefficient of performance (COP) defined as

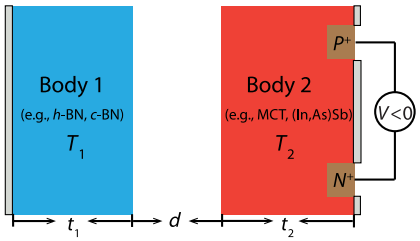

FIG. 1. Schematic of the configuration. The system consists of body 1 [material supporting surface-phonon polaritons such as hexagonal BN (*h*-BN) and cubic BN (*c*-BN)] and body 2 [a narrow-band-gap semiconductor such as (Hg,Cd)Te (MCT) and (In,As)Sb] in close proximity. The two bodies are backed by perfect electric conductor mirrors. Body 2 is under a negative bias V.

$$\mathrm{COP} = \frac{P \times \mathrm{area}}{I \times V} = \frac{P}{J \times V}, \tag{2}$$

where $J = I/\mathrm{area}$ with the area being the surface area of body 1 facing body 2. Since the net cooling power, which arises from the radiative exchange between the two bodies, scales linearly with the area defined here in Eq. (2), for convenience it is useful to define a current density as the total current divided by this area. The current density, thus, is defined in a normalized measure of the total current that passes through the device and does not necessarily correspond to the actual electric current density within the device.

Similar to the treatment in Ref. [28], we now present a simple analytical calculation of the negative luminescent device that highlights the essential physics. Using Eq. (1) and assuming that the heat exchange between the two bodies is narrow banded near the band-gap frequency $\omega_g = E_g/\hbar$, we can then define an apparent radiant temperature T_2^* by setting

$$\frac{\hbar\omega_g}{e^{\frac{\hbar\omega_g - qV}{k_B T_2}} - 1} = \frac{\hbar\omega_g}{e^{\frac{\hbar\omega_g}{k_B T_2^*}} - 1}, \tag{3}$$

and, hence,

$$T_2^* = T_2\left(1 - \frac{qV}{\hbar\omega_g}\right)^{-1}, \tag{4}$$

which is Eq. (5) in Ref. [11]. As far as the radiation properties are concerned, the semiconductor has an effective temperature T_2^* less than its thermodynamic temperature T_2 in the presence of a negative bias $V < 0$.

In order to achieve solid-state cooling of body 1, we must have $T_2^* < T_1$, and, therefore, the applied voltage must satisfy $V < V_t$, where the threshold voltage

$$V_t = \frac{\hbar\omega_g}{q}\frac{T_1 - T_2}{T_1}. \tag{5}$$

In the case of a substantial negative bias, the emission from the semiconductor body 2 can be ignored. Within the same narrow-banded approximation as discussed above, the cooling power density can then be estimated as

$$P_{\max} = \hbar\omega_g F_{1\to 2}, \tag{6}$$

where $F_{1\to 2}$ is the photon number flux from body 1 to body 2. Also, $J = -qF_{1\to 2}$. Therefore, for $V < V_t$, the COP in Eq. (2) is simplified to be

$$\mathrm{COP} = -\frac{\hbar\omega_g}{qV}. \tag{7}$$

According to the second law of thermodynamics, the COP should be bounded by the Carnot limit, i.e.,

$$\mathrm{COP} \leq \frac{T_1}{T_2 - T_1}. \tag{8}$$

From Eqs. (5) and (7), we see that the COP reaches the Carnot limit exactly when $V = V_t$, and falls below the Carnot limit when $V < V_t$. The dependence of the COP on the voltage can be understood from Eq. (7). Each photon traversing the vacuum gap removes energy of $\hbar\omega_g$ from body 1 at the cost of injected electric energy of qV into body 2. Therefore, the COP decreases as the magnitude of the applied voltage V increases.

We now illustrate the choice of materials and the operation regime for the device using the simple analytic model. In general, the photon flux from body 1 to body 2 is

$$F_{1\to 2} = \int_{\omega_g}^{+\infty} d\omega A(\omega) \frac{1}{e^{\hbar\omega/k_B T_1} - 1}, \tag{9}$$

where $A(\omega)$ is the spectral heat-transfer coefficient and $A(\omega) = A_0(\omega) = (\omega^2/4\pi^2c^2)$ if the two bodies are in the far field. The body 1 is a blackbody, and the absorption coefficient of body 2 is unity at frequencies above the band gap. $A(\omega)$ can be greater than $A_0(\omega)$ in the near-field case. In both near-field and far-field cases, suppose $\hbar\omega_g \gg k_B T_1$, Eq. (9) is approximated as

$$F_{1\to 2} = \int_{\omega_g}^{+\infty} d\omega A(\omega) e^{-\hbar\omega/k_B T_1} \propto e^{-\hbar\omega_g/k_B T_1}. \tag{10}$$

Therefore, in this case, the cooling power density is exponentially suppressed by the factor $e^{-\hbar\omega_g/k_B T_1}$. It follows that to have substantial cooling power density, we like to choose a narrow-band-gap semiconductor with $\hbar\omega_g$ on the order of $k_B T_1$. For operation around the room temperature of 300 K, the use of a narrow-band-gap semiconductor is, therefore, required.

A general thermal body will typically have its emissivity less than unity. Therefore, in applying Eq. (9) to a general thermal body in the far-field regime, we always have $A(\omega) < A_0(\omega)$. Therefore, in the far-field regime, the cooling power density is limited by the Stefan-Boltzmann limit of blackbody radiation. On the other hand, since in the near field the heat exchange can significantly exceed the Stefan-Boltzmann limit, the near-field regime represents an opportunity to significantly enhance the cooling power density achievable with negative luminescence.

III. ANALYSIS OF A NEAR-FIELD NEGATIVE LUMINESCENT REFRIGERATION DEVICE

A. Material systems and geometry

The discussion in Sec. II highlights the essential physics of negative luminescent refrigeration and points to the importance of performing such cooling in the near-field regime. Motivated by this discussion, here we present a detailed analysis of the system shown in Fig. 1. For the semiconductor (i.e., body 2 in Fig. 1), we use a narrow-band-gap semiconductor MCT. MCT is a commonly used material for infrared detector applications. With $x = 0.2$, it has a band gap of $E_g = 0.169$ eV. In our calculation, we choose the semiconductor to have a temperature of $T_2 = 300$ K. The band gap of MCT, therefore, equals a few times $k_B T_2 = 0.026$ eV. The dielectric constant of MCT as a function of frequency is taken from Ref. [29].

For the body to be cooled (i.e., body 1 in Fig. 1), we assume a temperature $T_1 = 290$ K and choose to use h-BN. h-BN is an anisotropic material with a uniaxial dielectric tensor as characterized by the ordinary and the extraordinary dielectric functions ϵ_o and ϵ_e, respectively. Both ϵ_o and ϵ_e have a resonance corresponding to an underlying phonon-polariton resonance. It is well known that the presence of surface-phonon polariton leads to significantly enhanced near-field thermal transfer [13], hence, the choice of h-BN in our case since its phonon-polariton frequency is well aligned with the band gap of MCT, corresponding to the wavelength of 7.3 μm. The phonon-polariton resonant wavelengths defined as the wavelengths where the imaginary parts of ϵ_o and ϵ_e maximize are located at 12.8 and 7.3 μm, respectively. The dielectric function of h-BN as a function of frequency is obtained from the model in Ref. [30].

In the calculation, the thicknesses of body 1 and body 2 denoted as t_1 and t_2 are chosen to be 5 μm to ensure significant emission and absorption. The two bodies are separated by a vacuum gap of size d, and both bodies are backed by perfect electric conductor mirrors. We consider only the case where the c axis of h-BN is perpendicular to the surface of body 1.

The setup here is a commonly used configuration for demonstrating near-field heat transfer through vacuum between two bodies. When two thermal bodies of different temperatures are brought in close proximity with separation below the thermal wavelength, the heat transfer between them can be enhanced beyond Planck's law of blackbody radiation due to the contributions from the evanescent waves [31–33]. Such enhancement is particularly prominent when the interacting bodies support surface modes, such as surface-plasmon polaritons or surface-phonon polaritons [22,34]. Similar to the scenario considered in our case, the heat transfer between a semiconductor and a polar material supporting surface-phonon polaritons has also been discussed in the context of thermophotovoltaics [13] as well as thermal rectification [35,36].

We also note that the choices of material for the two bodies are not limited to the materials considered here. Any combination of a material supporting surface resonant modes, such as surface-phonon polaritons or surface-plasmon polaritons, and a narrow-band-gap semiconductor whose band gap is below the corresponding

surface-polariton frequency can be used in the configuration for negative luminescent refrigeration. Either body can also have nanopatterning on the surface facing the vacuum gap to further enhance the transferred power density.

B. Computational methods

To evaluate the performance of the negative luminescent refrigeration device, we use the formalism of fluctuational electrodynamics [16,17,28,31,37,38]. In this formalism, one describes the heat transfer between objects by computing the electromagnetic flux resulting from fluctuating current sources inside each object. The cooling power density can then be obtained as [39,40]

$$P = P_{\text{ideal}} = \int_{\omega_g}^{+\infty} [\Theta(\omega, T_1, 0) - \Theta(\omega, T_2, V)]\Phi(\omega) d\omega. \quad (11)$$

In Eq. (11), $\Phi(\omega)$ is the sum of transmission factors at lateral wave vector $\boldsymbol{k}_\parallel$ at frequency ω, i.e.,

$$\Phi(\omega) = \frac{1}{2\pi} \sum_{j=s,p} \left\{ \int_0^{k_0} \frac{d^2\boldsymbol{k}_\parallel}{4\pi^2} \frac{(1-|r_j^{(1)}|^2)(1-|r_j^{(2)}|^2)}{|1 - r_j^{(1)} r_j^{(2)} e^{2ik_\perp d}|^2} + \int_{k_0}^{\infty} \frac{d^2\boldsymbol{k}_\parallel}{4\pi^2} \frac{4\text{Im}(r_j^{(1)})\text{Im}(r_j^{(2)})}{|1 - r_j^{(1)} r_j^{(2)} e^{2ik_\perp d}|^2} \right\}, \quad (12)$$

where $k_0 = \omega/c$ is the free-space wave vector, $\boldsymbol{k}_\parallel = (k_x, k_y)$, $k_\perp = \sqrt{k_0^2 - |\boldsymbol{k}_\parallel|^2}$ is the wave vector perpendicular the surfaces of body 1 and 2, $j = s,\ p$ accounts for the s and p polarizations, $r_j^{(1)}$ and $r_j^{(2)}$ are Fresnel reflection coefficients from vacuum to body 1 with perfect electric conductor (PEC) and from vacuum to body 2 with PEC for j polarization, respectively. For each ω in Eq. (12), the integrand peaks at the value of $\boldsymbol{k}_\parallel$ that corresponds to the dispersion relation $\omega(\boldsymbol{k}_\parallel)$ of the surface-phonon polariton [35,36]. The heat transfer in the near field is, therefore, strongly dominated by the contributions from surface-phonon polaritons.

A semiconductor that is ideal for negative luminescent refrigeration should have entire emission arising from electron-hole recombination. An ideal semiconductor, therefore, should have emission only at frequencies above the band-gap frequency. Moreover, the recombination should be completely radiative. In the ideal case, the current density J_{ideal} is

$$J = J_{\text{ideal}} = q \int_{\omega_g}^{+\infty} \left[\frac{\Theta(\omega, T_2, V)}{\hbar\omega} - \frac{\Theta(\omega, T_1, 0)}{\hbar\omega} \right] \Phi(\omega) d\omega, \quad (13)$$

from which the COP can then be obtained using Eq. (2).

In the scheme considered here, the inherent material nonidealities are the existence of significant nonradiative recombination, such as Auger recombination, as well as sub-band-gap thermal radiation. In the presence of nonradiative recombination, the total current density now has contributions from both radiative and nonradiative recombination, i.e.,

$$J = q(J_{\text{ideal}} + R), \quad (14)$$

where R is the nonradiative recombination rate per unit surface area, and then COP can be obtained by combining Eqs. (2) and (14).

The net sub-band-gap heat flow is from the hot body 2 to the cold body 1 and, therefore, represents a parasitic process that is detrimental for the objective of cooling here. In the presence of free-carrier thermal radiation, the net sub-band-gap heat flow from body 2 to body 1 is expressed as

$$P_s = \int_0^{\omega_g} [\Theta(\omega, T_2, 0) - \Theta(\omega, T_1, 0)]\Phi(\omega, V) d\omega. \quad (15)$$

Here, since the density of free carriers of the semiconductor depends on the voltage, the dielectric function of the semiconductor in the sub-band-gap wavelength range, thus, also depends on the voltage. $\Phi(\omega, V)$ is computed with a voltage correction included. The overall net cooling power density is

$$P = P_{\text{ideal}} - P_s, \quad (16)$$

and the COP can be obtained by combining Eqs. (2), (14), and (16).

The objectives of our calculation here are to illustrate the theoretical limit of the performance using the ideal case and to consider the impact of the most fundamental nonidealities on the performance of the device. In the following, we first discuss the ideal case in Sec. III C. We then discuss nonradiative recombination and sub-band-gap radiation in Secs. III D and III E, respectively.

C. Ideal case

We consider the ideal case first. In the absence of nonradiative recombination and sub-band-gap free-carrier thermal radiation, we use Eqs. (11) and (12) to compute the cooling power P and the current density J, respectively, and then obtain the COP with Eq. (2).

The net cooling power densities P as a function of the magnitude of the bias for $d = 10$, 100, 1000 nm are shown in Fig. 2(a). For each d, when $V = 0$, the temperature difference between the bodies results in net heat flow from body 2 to body 1, and, thus, a negative value of P. Applying a negative voltage to body 2, i.e., having a negative V, results in the suppression of the radiation from body 2 and, hence, the increase of the cooling power density P. When $V < V_t$, the apparent temperature of body 2 becomes lower

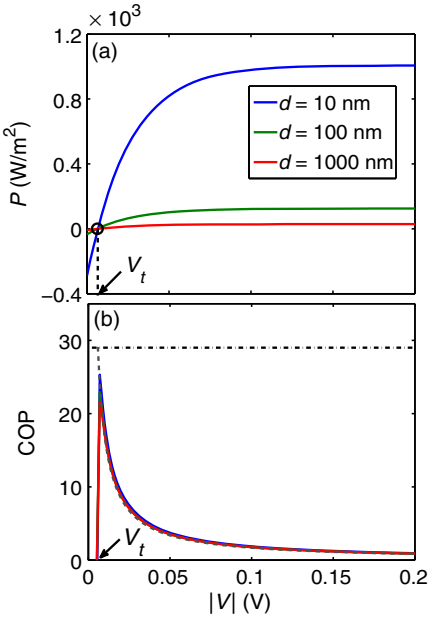

FIG. 2. (a) Net cooling power density and (b) COP as a function of the magnitude of the reverse bias. The blue, green, and red curves are for $d = 10$, 100, 1000 nm, respectively. The threshold voltage V_t is labeled in both figures. In (b), the horizontal dotted line represents the Carnot efficiency, and the gray dashed curve is the COP obtained using Eq. (7).

than that of body 1, and, thus, P becomes positive. As indicated in Fig. 2, in the ideal case considered here this threshold voltage V_t is independent of the gap size d. The value of $V_t = -0.0065$ V, as obtained from simulation, compares reasonably well with the prediction of $V_t = -0.0058$ V as obtained from the results of the simple analytical model described in Eq. (5). When the magnitude of V is sufficiently large, the heat flux from body 2 to 1 becomes negligible for the temperatures considered here, and, therefore, P saturates to the heat flux from body 1 to 2. As d decreases from 1000 to 10 nm, the maximum cooling power density increases from 29.3 to 1007.0 W/m^2. As a comparison, the maximum power density in the far-field limit for this system is 11.5 W/m^2. Operating in the near-field regime, therefore, significantly increases the cooling power density beyond the far-field limit.

In Fig. 2(b), we show the COP for the three gap separations. For all gap sizes, at $V = V_t$, the COP is zero as expected since the net cooling power density is zero. As V decreases below V_t, the COP quickly maximizes as then decreases as V further decreases. The COP is largely independent of the gap size. Except for the regime near V_t, the COP agrees very well with the analytical model results of Eq. (7) shown as the gray dashed line in Fig. 2(b). For $d = 10$ nm, the maximum COP is 25.3, which can be compared with the Carnot efficiency limit of 29 for this system. In this ideal case, the device can operate with very high efficiency.

The result in this section shows that in the absence of material nonidealities, the device shown in Fig. 1 can perform with a high COP close to the Carnot limit, as well as a high cooling power density far exceeding the far-field limit by operating in the near field. In what follows, we evaluate how the inherent nonidealities of the semiconductor influence the device performance.

D. Auger recombination

The analysis in Sec. III C assumes that the only carrier generation or recombination mechanism in the semiconductor is completely radiative. On the other hand, for narrow-band-gap semiconductors such as MCT, there is significant Auger recombination which is nonradiative. In this section, we evaluate the impact of Auger processes. The rate of net Auger recombination R in Eq. (14) takes the form [41,42]

$$R = C_0 n_i^3 \left[\exp\left(\frac{3qV}{2k_B T}\right) - 1\right] t_2, \tag{17}$$

where C_0 is the Auger recombination coefficient, n_i is the intrinsic carrier density, and t_2 is the thickness of the semiconductor. For MCT, $n_i = 2.614 \times 10^{16}$ cm^{-3} is calculated using Eq. (1) in Ref. [43] and $C_0 = 4.88 \times 10^{-26}$ cm^6 s^{-1} is inferred from the carrier lifetime data in Ref. [44]. The first and second terms in the brackets of Eq. (17) arise from recombination and generation processes, respectively.

In Fig. 3(a) we plot R as a function of the magnitude of the reverse bias. At $V = 0$, the semiconductor is at equilibrium, and the net Auger recombination rate is zero since the generation rate balances the recombination rate as shown in Eq. (17). With a large enough negative bias, the net recombination rate saturates to a large negative value. In such a case, the application of large negative bias suppresses the carrier density and, hence, suppresses carrier recombination. As a result, there is a net generation of carriers in the system, which is represented by a net negative recombination rate.

The presence of Auger recombination does not affect the cooling power since it occurs in body 2. This can be seen from the formalism in Sec. III B. On the other hand, the cooling power at large negative voltages is given by the radiation from body 1 to body 2. Therefore, the cooling power is the same as Fig. 2(a) even in the presence of Auger generation given that the temperature of body 2 is maintained constant.

Auger recombination, on the other hand, significantly degrades the COP. We compute the COP using Eqs. (2), (11), and (14). Figure 3(b) shows the COP as a function of the magnitude of voltage for $d = 10$, 100, 1000 nm in blue, green, and red curves, respectively. Comparing Fig. 3(b) with Fig. 2(b), we see that the COP is degraded by several orders of magnitude as compared to the ideal case. In this

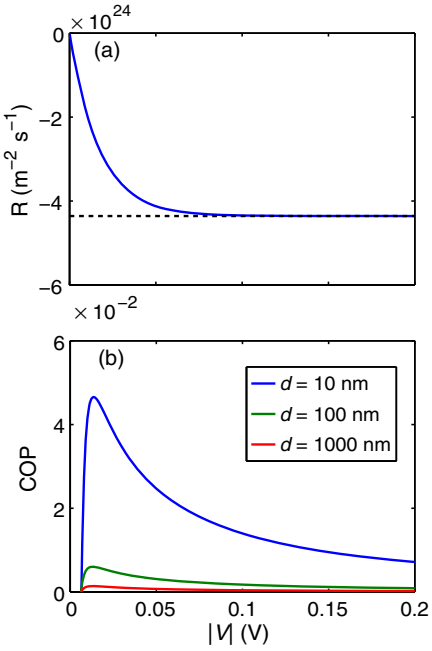

FIG. 3. (a) The net Auger recombination rate as a function of the magnitude of the reverse bias. The generation rate is plotted as the black dashed line. (b) COP as a function of the magnitude of the reverse bias in the presence of Auger recombination for $d = 10$, 100, 1000 nm in blue, green, and red curves, respectively.

case, the COP increases in the near field, since operating in the near field enhances radiative recombination and, hence, enhances internal quantum efficiency for the radiative processes in body 2.

E. Sub-band-gap thermal radiation

For a narrow-band-gap semiconductor with high intrinsic carrier density, the free carrier can result in a large thermal emission in the sub-band-gap wavelength regime. Such sub-band-gap heat transfer is detrimental since it results in a heat flow from the hot to the cold bodies. On the other hand, the free-carrier density can be suppressed using negative bias. In this section, we discuss the sub-band-gap heat transfer at long wavelengths.

To model the free-carrier absorption, for simplicity, in the frequency range below the band gap of MCT, we assume a Drude dielectric function [45]

$$\epsilon(\omega) = 1 - \frac{N_e q^2/\epsilon_0 m_e^*}{\omega^2 + i\omega\gamma_e} - \frac{N_h q^2/\epsilon_0 m_h^*}{\omega^2 + i\omega\gamma_h}, \qquad (18)$$

where N_e (N_h) and m_e^* (m_h^*) are the concentration and the effective mass of electrons (holes), respectively, γ_e (γ_h) is the damping rate of the electron (hole) plasma oscillation, and ϵ_0 is the vacuum permittivity. For MCT with $x \approx 0.2$, $m_e^* = 0.0114 m_0$, and $m_i^* = 0.55 m_0$ [46], where m_0 is the electron mass. γ_e and γ_h are related to the mobilities of electrons (μ_e) and holes (μ_h) through $\gamma_e = q/m_e^*\mu_e$, $\gamma_h = q/m_h^*\mu_e$, where $\mu_e = 1.0 \times 10^4$ cm^2/(V s), $\mu_h = 100$ cm^2/(V s) [46]. In the presence of a bias V, the N_e and N_h scale exponentially as a function of V expressed as $N_e = N_h = n_i \exp[qV/(2k_BT)]$. We also assume the mobilities are independent of V. For h-BN, here we again use the dielectric function model described by Eq. (1) in Ref. [30].

In evaluating the integral of Eq. (15), which is used for calculating the sub-band-gap heat transfer, instead of integrating in frequency from 0 to ω_g, we integrate between a narrower frequency range from 3.77×10^{13} rad/s to 2.13×10^{14} rad/s, corresponding to the wavelengths range between 50 and 8.86 μm. This is sufficient to capture most of the contributions to sub-band-gap heat exchange while reducing the computational cost. Having obtained the sub-band-gap heat transfer, the cooling power is then obtained from Eq. (16). In the section here, we also take into account Auger recombination by using Eq. (14) to compute the current density. From this, the COP is then computed using Eq. (2).

We show the net cooling power density as a function of the magnitude of the reverse bias for $d = 10$, 100, 1000 nm in Fig. 4(a) in blue, green, and red curves, respectively. In all three cases, cooling can be achieved with a negative bias having a sufficiently large magnitude. Unlike the ideal case, however, the threshold voltage in this case does depend on the spacing d. As d decreases, the sub-band-gap heat transfer increases faster than that of above-band-gap heat transfer, and, therefore, a larger reverse bias is needed for the device to reach the threshold condition. At $d = 10$ nm, the net cooling power density can reach 1006.4 W/m^2 at $V = -0.2$ V. When the magnitude of V is sufficiently large, the free-carrier density is strongly suppressed, and the net cooling power density approaches the ideal case, as can be seen from Fig. 4(a).

In Fig. 4(b), the COP as a function of the magnitude of the voltage for $d = 10$, 100, 1000 nm is shown in blue, green, and red curves, respectively. Compared to Fig. 3(b), since the net cooling power density is degraded by the presence of sub-band-gap heat transfer, the COP is much lower for most of the values of the bias voltage. On the other hand, since the decrease of V results in the suppression of the sub-band-gap heat transfer, when the magnitude of V is sufficiently large, the COP becomes close to that in Fig. 3(b). Therefore, for a large $|V|$, the COP is limited by the Auger recombination. We also note that the voltages applied in the p-n junction are in the reverse direction and serve to reduce the density of free carriers. However, for real material with defects, the carrier density is unlikely to reach an ideal limit, and, thus, the COP is far lower than the Carnot limit.

In addition to cooling power and COP, another metric to measure a cooling scheme is the equilibrium temperature that body 1 can reach when a negative bias is applied to the

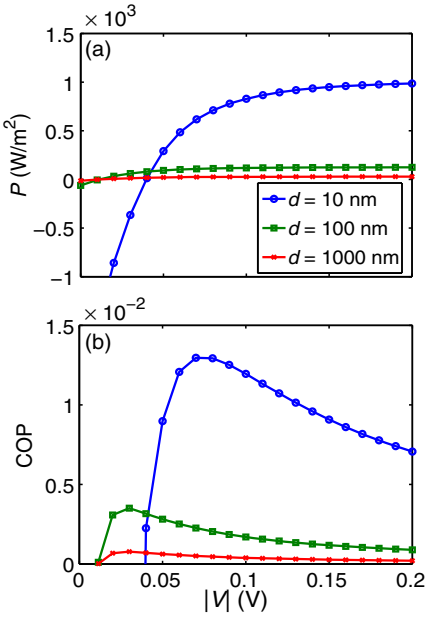

FIG. 4. (a) The net cooling power density as a function of the magnitude of the voltage in the presence of sub-band-gap heat transfer for $d = 10$, 100, 1000 nm in blue, green, and red curves, respectively. (b) The COP as a function of the magnitude of the voltage for $d = 10$, 100, 1000 nm with both Auger recombination and sub-band-gap heat transfer included.

p-n junction in body 2. In this system, assuming that body 1 undergoes heat exchange only with body 2 with no other parasitic heat loss mechanism and body 2 is maintained at a temperature of 300 K with an applied voltage on body 2 of −0.2 V, and with a 10-nm gap between the bodies, the equilibrium temperature of body 1 is estimated at 226 K by a self-consistent calculation that determines the temperature through power balance. This calculation does not take into account the variation of material properties with respect to the temperature. Nevertheless, the estimate does indicate that significant cooling in terms of temperature reduction can be achieved in this device.

To briefly summarize this section, in the proposed scheme for near-field negative luminescent refrigeration as considered here, the cooling power can reach the radiative limit as defined solely by the radiative heat exchange of the two bodies, in spite of Auger recombination and sub-band-gap heat radiation from free carriers that typically occur in narrow-band-gap semiconductors. The COP in this scheme is limited by the Auger recombination, again independent from the sub-band-gap heat radiation from the free carriers, since such radiation is suppressed at a negative bias with sufficiently large bias.

IV. CONCLUSION

In this paper, we propose a negative luminescent refrigeration device based on near-field electromagnetic heat exchange between a semiconductor under reverse bias and a polar material that supports surface-phonon polaritons. The power density of this cooling effect is significantly enhanced in the near-field regime. In the ideal case, the device can operate close to the Carnot limit with a large cooling power density around 10^3 W/m^2 at a gap separation of 10 nm. We further discuss the impacts of nonidealites on the performance of the device. In the presence of strong Auger recombination, such high cooling power density persists. Even with sub-band-gap free-carrier thermal radiation included, the cooling power density can still be achieved close to its maximum with a sufficiently large reverse bias. The performance and the robustness to nonidealities of this scheme are important to solid-state cooling applications.

Admittedly, the cooling power density and efficiency achieved by our device is lower than those of commercial thermoelectric coolers. However, due to the absence of direct contact between bodies, our device supports much faster temperature modulation than that of a thermoelectric cooler. For example, when the *h*-BN is only 100 nm, the maximum cooling power density at $T_1 = T_2 = 300$ K is 1171.3 W/m^2. Given that *h*-BN has a specific heat capacity of 0.8 J/(g K) [47] and a density of 2.18 g/cm^3 [47], the temperature slew rate is 6716 K/s, which is significantly faster than commercial Peltier coolers and even microdevice coolers designed for fast response times [48]. This allows the rapid modulation of temperatures which can benefit applications such as chip hot-spot cooling and life science applications [48].

ACKNOWLEDGMENTS

This work is supported by the Department of Energy "Light-Material Interactions in Energy Conversion" Energy Frontier Research Center under Grant No. DE-SC0001293.

[1] C. H. Henry and R. F. Kazarinov, Quantum noise in photonics, Rev. Mod. Phys. **68**, 801 (1996).
[2] W. W. Bewley, M. J. Jurkovic, C. L. Felix, J. R. Lindle, I. Vurgaftman, J. R. Meyer, E. H. Aifer, J. E. Butler, S. P. Tobin, P. W. Norton, and M. A. Hutchins, HgCdTe photodetectors with negative luminescent efficiencies > 80%, Appl. Phys. Lett. **78**, 3082 (2001).
[3] W. W. Bewley, J. R. Lindle, I. Vurgaftman, J. R. Meyer, J. L. Johnson, M. L. Thomas, and W. E. Tennant, Negative luminescence with 93% efficiency from midwave infrared HgCdTe diode arrays, Appl. Phys. Lett. **83**, 3254 (2003).
[4] T. Ashley, C. Elliott, N. Gordon, R. Hall, A. Johnson, and G. Pryce, Negative luminescence from $In_{1-x}Al_xSb$ and $Cd_xHg_{1-x}Te$ diodes, Infrared Phys. Technol. **36**, 1037 (1995).
[5] G. R. Nash, M. K. Ashby, J. R. Lindle, N. T. Gordon, W. W. Bewley, J. R. Meyer, J. Giess, L. Haworth, and T. Ashley, Long wavelength infrared negative luminescent devices

with strong auger suppression, J. Appl. Phys. **94**, 7300 (2003).
[6] T. Ashley, N. T. Gordon, G. R. Nash, C. L. Jones, C. D. Maxey, and R. A. Catchpole, Long-wavelength HgCdTe negative luminescent devices, Appl. Phys. Lett. **79**, 1136 (2001).
[7] D. Hoffman, A. Hood, Y. Wei, A. Gin, F. Fuchs, and M. Razeghi, Negative luminescence of long-wavelength InAs/GaSb superlattice photodiodes, Appl. Phys. Lett. **87**, 201103 (2005).
[8] A. Krier, *Mid-Infrared Semiconductor Optoelectronics* (Springer, Lancaster, UK, 2006).
[9] J. R. Lindle, W. W. Bewley, I. Vurgaftman, J. R. Meyer, J. L. Johnson, M. L. Thomas, E. C. Piquette, W. E. Tennant, E. P. Smith, and S. M. Johnson, HgCdTe negative luminescence devices for cold shielding and other applications, J. Electron. Mater. **35**, 1391 (2006).
[10] T. Ashley, C. Elliott, N. Gordon, T. Phillips, and R. Hall, Applications of negative luminescence, Infrared Phys. Technol. **38**, 145 (1997).
[11] P. Berdahl, Radiant refrigeration by semiconductor diodes, J. Appl. Phys. **58**, 1369 (1985).
[12] P. Berdahl, V. Malyutenko, and T. Morimoto, Negative luminescence of semiconductors, Infrared Phys. **29**, 667 (1989).
[13] A. Narayanaswamy and G. Chen, Surface modes for near field thermophotovoltaics, Appl. Phys. Lett. **82**, 3544 (2003).
[14] C. Luo, A. Narayanaswamy, G. Chen, and J. D. Joannopoulos, Thermal Radiation from Photonic Crystals: A Direct Calculation, Phys. Rev. Lett. **93**, 213905 (2004).
[15] B. Guha, C. R. Otey, C. B. Poitras, S. Fan, and M. Lipson, Near-field radiative cooling of nanostructures, Nano Lett. **12**, 4546 (2012).
[16] M. Krüger, T. Emig, and M. Kardar, Nonequilibrium Electromagnetic Fluctuations: Heat Transfer and Interactions, Phys. Rev. Lett. **106**, 210404 (2011).
[17] C. R. Otey and S. Fan, Numerically exact calculation of electromagnetic heat transfer between a dielectric sphere and plate, Phys. Rev. B **84**, 245431 (2011).
[18] R. Messina and M. Antezza, Casimir-Lifshitz force out of thermal equilibrium and heat transfer between arbitrary bodies, Europhys. Lett. **95**, 61002 (2011).
[19] A. Narayanaswamy and G. Chen, Thermal near-field radiative transfer between two spheres, Phys. Rev. B **77**, 075125 (2008).
[20] A. W. Rodriguez, M. T. Homer Reid, J. Varela, J. D. Joannopoulos, F. Capasso, and S. G. Johnson, Anomalous Near-Field Heat Transfer between a Cylinder and a Perforated Surface, Phys. Rev. Lett. **110**, 014301 (2013).
[21] C. R. Otey, L. Zhu, S. Sandhu, and S. Fan, Fluctuational electrodynamics calculations of near-field heat transfer in non-planar geometries: A brief overview, J. Quant. Spectrosc. Radiat. Transfer **132**, 3 (2014).
[22] A. I. Volokitin and B. N. J. Persson, Near-field radiative heat transfer and noncontact friction, Rev. Mod. Phys. **79**, 1291 (2007).
[23] R. S. Ottens, V. Quetschke, S. Wise, A. A. Alemi, R. Lundock, G. Mueller, D. H. Reitze, D. B. Tanner, and B. F. Whiting, Near-Field Radiative Heat Transfer between Macroscopic Planar Surfaces, Phys. Rev. Lett. **107**, 014301 (2011).
[24] S. Shen, A. Narayanaswamy, and G. Chen, Surface phonon polaritons mediated energy transfer between nanoscale gaps, Nano Lett. **9**, 2909 (2009).
[25] E. Rousseau, A. Siria, G. Jourdan, S. Volz, F. Comin, J. Chevrier, and J. J. Greffet, Radiative heat transfer at the nanoscale, Nat. Photonics **3**, 514 (2009).
[26] A. Kittel, W. Müller-Hirsch, J. Parisi, S. A. Biehs, D. Reddig, and M. Holthaus, Near-Field Heat Transfer in a Scanning Thermal Microscope, Phys. Rev. Lett. **95**, 224301 (2005).
[27] R. St-Gelais, B. Guha, L. Zhu, S. Fan, and M. Lipson, Demonstration of strong near-field radiative heat transfer between integrated nanostructures, Nano Lett. **14**, 6971 (2014).
[28] K. Chen, P. Santhanam, S. Sandhu, L. Zhu, and S. Fan, Heat-flux control and solid-state cooling by regulating chemical potential of photons in near-field electromagnetic heat transfer, Phys. Rev. B **91**, 134301 (2015).
[29] E. Palik, *Handbook of Optical Constants of Solids* (Academic, New York, 1985).
[30] R. Geick, C. H. Perry, and G. Rupprecht, Normal modes in hexagonal boron nitride, Phys. Rev. **146**, 543 (1966).
[31] D. Polder and M. Van Hove, Theory of radiative heat transfer between closely spaced bodies, Phys. Rev. B **4**, 3303 (1971).
[32] J. B. Pendry, Radiative exchange of heat between nanostructures, J. Phys. Condens. Matter **11**, 6621 (1999).
[33] J. J. Loomis and H. J. Maris, Theory of heat transfer by evanescent electromagnetic waves, Phys. Rev. B **50**, 18517 (1994).
[34] O. Ilic, M. Jablan, J. D. Joannopoulos, I. Celanovic, and M. Soljačić, Overcoming the black body limit in plasmonic and graphene near-field thermophotovoltaic systems, Opt. Express **20**, A366 (2012).
[35] L. P. Wang and Z. M. Zhang, Thermal rectification enabled by near-field radiative heat transfer between intrinsic silicon and a dissimilar material, Nanoscale Micro. Thermophys. Eng. **17**, 337 (2013).
[36] P. J. van Zwol, K. Joulain, P. Ben-Abdallah, and J. Chevrier, Phonon polaritons enhance near-field thermal transfer across the phase transition of VO_2, Phys. Rev. B **84**, 161413 (2011).
[37] S. M. Rytov, *Theory of Electric Fluctuations and Thermal Radiation* (Air Force Cambridge Research Center, Bedford, MA, 1959).
[38] W. C. Chew, *Waves and Fields in Inhomogeneous Media* (IEEE, New York, 1995).
[39] J. Dai, S. A. Dyakov, and M. Yan, Enhanced near-field radiative heat transfer between corrugated metal plates: Role of spoof surface plasmon polaritons, Phys. Rev. B **92**, 035419 (2015).
[40] M. Francoeur, M. P. Menguc, and R. Vaillon, Spectral tuning of near-field radiative heat flux between two thin silicon carbide films, J. Phys. D **43**, 075501 (2010).
[41] T. Tiedje, E. Yablonovitch, G. Cody, and B. Brooks, Limiting efficiency of silicon solar cells, IEEE Trans. Electron Devices **31**, 711 (1984).

[42] S. Sandhu, Z. Yu, and S. Fan, Detailed balance analysis of nanophotonic solar cells, Opt. Express **21**, 1209 (2013).

[43] J. L. Schmit, Intrinsic carrier concentration of $Hg_{1-x}Cd_xTe$ as a function of x and T using $\boldsymbol{k}$-$\boldsymbol{p}$ calculations, J. Appl. Phys. **41**, 2876 (1970).

[44] P. E. Petersen, Auger recombination in $Hg_{1-x}Cd_xTe$, J. Appl. Phys. **41**, 3465 (1970).

[45] C. Fu and Z. Zhang, Nanoscale radiation heat transfer for silicon at different doping levels, Int. J. Heat Mass Transfer **49**, 1703 (2006).

[46] A. M. Itsuno, Ph.D. dissertation, University of Michigan, 2012.

[47] I. P.-T. Institute, NSM archive—Physical properties of semiconductors, 1998.

[48] H. Bottner, in Proceedings of the 24th ICT, 2005, pp. 1–8.